

# Directed transport of two interacting particles in a washboard potential

D. Hennig, A. D. Burbanks, and A. H. Osbaldestin

*Department of Mathematics, University of Portsmouth, Portsmouth, PO1 3HF, UK*

## Abstract

We study the conservative and deterministic dynamics of two nonlinearly interacting particles evolving in a one-dimensional spatially periodic washboard potential. A weak tilt of the washboard potential is applied biasing one direction for particle transport. However, the tilt vanishes asymptotically in the direction of bias. Moreover, the total energy content is not enough for both particles to be able to escape simultaneously from an initial potential well; to achieve transport the coupled particles need to interact cooperatively. For low coupling strength the two particles remain trapped inside the starting potential well permanently. For increased coupling strength there exists a regime in which one of the particles transfers the majority of its energy to the other one, as a consequence of which the latter escapes from the potential well and the bond between them breaks. Finally, for suitably large couplings, coordinated energy exchange between the particles allows them to achieve escapes — one particle followed by the other — from consecutive potential wells resulting in directed collective motion. The key mechanism of transport rectification is based on the asymptotically vanishing tilt causing a symmetry breaking of the non-chaotic fraction of the dynamics in the mixed phase space. That is, after a chaotic transient, only at one of the boundaries of the chaotic layer do resonance islands appear. The settling of trajectories in the ballistic channels associated with transporting islands provides long-range directed transport dynamics of the escaping dimer.

PACS numbers: 05.60.Cd, 05.45.Ac, 05.60.-k, 05.45.Pq

## I. INTRODUCTION

The study of transport phenomena has attracted considerable interest over the years due to its relevance in many physical situations. The latter are often described on the basis of one-dimensional particle motion in a tilted spatially periodic potential [1]-[13]. Corresponding experimental realisations include Josephson junctions [14], charge density waves [15], superionic conductors [16], rotation of dipoles in external fields [17], phase-locked loops [18] and diffusion of dimers on surfaces [7, 8, 9, 19, 20, 21, 22, 23] to name but a few. In many of these aforementioned situations the particles, in addition to their motion in the periodic potential, interact, which may lead to cooperative effects not found in situations of individual particle motion [24]-[27].

The objective of the current work is to investigate the conditions under which it is possible to generate a directed flow along with collective motion in a system of coupled particles. To be precise, we study the transport of a dimer evolving in a washboard potential experiencing a weak tilt force. The nonlinear bond dynamics between the two monomers, constituting the dimer, is modelled by a Morse potential allowing for bond breaking, i.e. fragmentation. We focus our interest on the chaos-promoted detrapping mechanism for dimers that initially reside in one well of the washboard potential. Provided that such a detrapping transition happens the question then is under which circumstances subsequent directed long-range particle transport is achievable. Since the total system energy is too low for both monomers to be able to escape from the potential well simultaneously, we explore whether cooperative energy redistribution is possible allowing at least one of the monomers to escape and subsequently display directed motion. We also elucidate the possible scenario in which the energy exchange between the monomers proceeds in such a well-coordinated manner that the monomers move separately from one well into the next, one following the other, resulting in directed motion of the dimer.

The paper is organised as follows: In the next section the model of the dimer system is introduced, followed by the formulation of the escape problem together with a brief discussion of the related phase space structure. In Section III the particle current is studied and the occurrence of different transport scenarios is described. Afterwards in Section IV we relate the phase space dynamics to the regime of high particle current. In particular chaotic invariant sets, their connection with singularities of the escape time function, and their

relevance for the escape process are considered. In Section V we present an alternative description of the escape problem as the motion of a single particle in a two-dimensional potential landscape. Finally we summarise and discuss our results.

## II. THE MODEL OF THE DIMER SYSTEM

We study the dimer dynamics with a Hamiltonian of the following form

$$H = \sum_{n=1}^2 \left[ \frac{p_n^2}{2} + U_0(q_n) + U_1(q_n) \right] + H_{int}(q_1, q_2), \quad (1)$$

wherein  $p_n$  and  $q_n$ ,  $n = 1, 2$ , denote the canonically conjugate momenta and positions of the two coupled particles of unit mass evolving in the periodic, spatially-symmetric washboard potential of unit period given by

$$U_0(q) = U_0(q + 1) = -\frac{\cos(2\pi q)}{2\pi}. \quad (2)$$

The external field

$$U_1(q) = -F(q - \log[\cosh(q - q_0)]) \quad (3)$$

exerts a tilt on the washboard potential. The potential is sketched in Fig. 1 for tilt strength  $F = 0.01$ . The value of the parameter  $q_0 = 10$  in the second term on the right hand side of Eq. (3) is chosen such that the tilt rapidly diminishes when the coordinate  $q$  exceeds  $q_0$  and eventually upon further growth of  $q$  the bias vanishes. On the other hand as long as  $q \ll q_0$  the tilt adopts the value  $2F$ . Therefore particles that manage to escape from a potential well into the *asymptotic region*  $q_0 < q \rightarrow \infty$  experience only a finite acceleration period at the end of which any forward motion must proceed unbiased. The question then arises whether escaping particles carry on moving forward even in the range where the bias is no longer present.

The interaction part of the Hamiltonian  $H_{int}$  given by

$$H_{int} = \frac{D}{2} (1 - \exp[-\alpha(q_2 - q_1 - l_0)])^2, \quad (4)$$

is responsible for the coupling between the monomers which results from a Morse interaction potential of depth  $D$ , where  $\alpha$  is the range parameter and the parameter  $l_0$  denotes the equilibrium distance between the monomers. Throughout the paper we chose  $l_0 = 0.5$ , i.e. the equilibrium distance amounts to half the length of one period of the washboard potential.

The equations of motion are

$$\begin{aligned}\ddot{q}_1 &= -\sin(2\pi q_1) + F(1 - \tanh(q_1 - q_0)) \\ &\quad + \alpha D(1 - \exp[-\alpha(q_2 - q_1 - l_0)]) \exp[-\alpha(q_2 - q_1 - l_0)]\end{aligned}\tag{5}$$

$$\begin{aligned}\ddot{q}_2 &= -\sin(2\pi q_2) + F(1 - \tanh(q_2 - q_0)) \\ &\quad - \alpha D(1 - \exp[-\alpha(q_2 - q_1 - l_0)]) \exp[-\alpha(q_2 - q_1 - l_0)].\end{aligned}\tag{6}$$

The interaction strength between the two monomers is effectively determined by the product  $\alpha D$ . For  $\alpha D = 0$  the system decouples into two integrable subsystems and the dynamics is characterised by individual regular monomer motions in the washboard potential. For nonzero  $\alpha D$  the dynamics is no longer integrable. To prevent unphysical events in which the left monomer overtakes the right one, a sufficiently strong coupling between them is required. The choice  $\alpha = 3$  and  $D \in [0.5, 3]$  ensures that. On the other hand the effective coupling strength,  $\alpha D \in [1.5, 9]$ , is then too large by far to treat the coupling using a perturbational approach. We therefore resort to a numerical analysis of the coupled monomer dynamics.

Let us briefly discuss the phase space structure corresponding to the dynamics in the tilted washboard potential. In the range  $-\infty < q \lesssim 10$  the tilt force,  $-dU_1/dq$ , is effectively of strength  $2F$ . For uncoupled monomers ( $\alpha D = 0$ ) there exist saddles at  $q_s^k = 0.5 + k - \arcsin(2F)/(2\pi)$  and centers at  $q_c^k = k - \arcsin(2F)/(2\pi)$  for integer values  $k$ . For very small tilt strength  $F \lesssim 0.01$  the barrier height of the washboard potential, given by the difference between the energy of the saddle and the center, is virtually equivalent to those of the corresponding unbiased system with  $F = 0$ , i.e.  $E_b \simeq 1/\pi$ .

### III. PARTICLE CURRENT

In this section we consider the emergence of a particle current. The initial positions of the monomers are taken as  $-q_1(0) = q_2(0) = 0.25$ , so that the dimer is contained in one of the wells of the washboard potential and, for the weak tilt strength  $F = 0.01$  used throughout the paper, is initially situated in virtually the lowest energy dimer configuration compatible with the bond length  $l_0$ . The dimer initially has potential energy  $E_{pot} = \sum_{n=1,2}[U_0(q_n) + U_1(q_n)] = 0.3221$  which is of the order of the barrier energy  $E_b \simeq 1/\pi \simeq 0.3183$  of the washboard potential. Note that since the bond between the monomers is initially undistorted, the contribution from the Morse potential energy  $H_{int}$  to the system's initial potential energy

is zero. The initial kinetic energy of the dimer is taken as  $E_{kin} = 0.1234$ . Crucially the total energy  $E_{total} = 0.4455 < 2E_b$  is not sufficient that the two monomers can escape simultaneously from a well of the washboard potential. In order for directed motion of the dimer to occur at all, cooperation between the monomers, in the form of appropriately coordinated energy exchanges, is required.

Particle transport is assessed quantitatively by the mean momentum, viz. the *current*, which is defined as the time average of the ensemble averaged momentum, i.e.

$$p = \frac{1}{T_s} \int_0^{T_s} dt' \langle p_1(t') + p_2(t') \rangle, \quad (7)$$

with simulation time  $T_s$  and with the ensemble average given by

$$\langle p_i(t) \rangle = \frac{1}{N} \sum_{n=1}^N p_{i,n}(t), \quad i = 1, 2. \quad (8)$$

Here  $N$  denotes the number of particles constituting the ensemble. For the computation of the ensemble average, trajectories belonging to  $N = 2 \times 10^5$  values of the pair of initial momenta  $(p_1(0), p_2(0))$  are taken. These initial values are uniformly distributed on an iso-energetic ring in the  $p_1 - p_2$ -plane such that the relation

$$2E_{kin} = p_1^2 + p_2^2 \quad (9)$$

is fulfilled. Notice the symmetry  $p_i \leftrightarrow -p_i$  and  $i = 1, 2$ . Hence there is no bias contained in the ensemble of initial conditions. The simulation time interval is  $T_s = 10^5$  being equivalent to almost  $4 \times 10^4$  the period duration for harmonic oscillations near the bottom of a potential well.

In what follows we vary the depth of the Morse potential,  $D$ , playing, for fixed  $\alpha = 3$ , the role of the coupling parameter. The dependence of the current, defined in Eqs. (7) and (8), on the value of  $D$  is shown in Fig. 2. For values  $D \lesssim 3.9$  the current exhibits variations and even vanishes for  $D = 1.1$ . Interestingly the current effectively grows for  $d \gtrsim 1.2$ . Finally the current rises rapidly and monotonically in the range  $3.9 \lesssim D \lesssim 4.5$  and effectively saturates at a high level for  $D \gtrsim 4.5$ . We emphasise that the amplitude of the tilt force  $F = 0.01$  is too small to alter the washboard potential significantly compared to the case without tilt. In fact the influence of the tilt force is sufficiently small that, for example, the potential barrier immediately to the right of the initial well is lowered by a mere 7.5% and hence the induced bias is very weak.

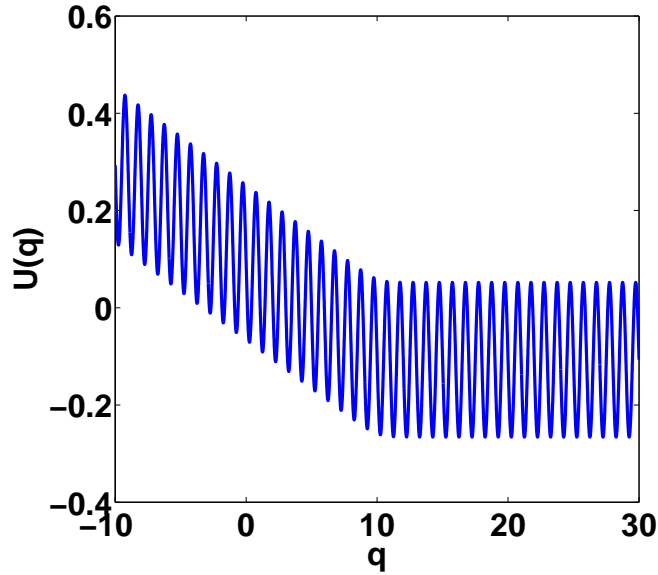


Figure 1: The potential  $U(q) = U_0(q) + U_1(q)$  for parameter values  $F = 0.01$  and  $q_0 = 10$ .

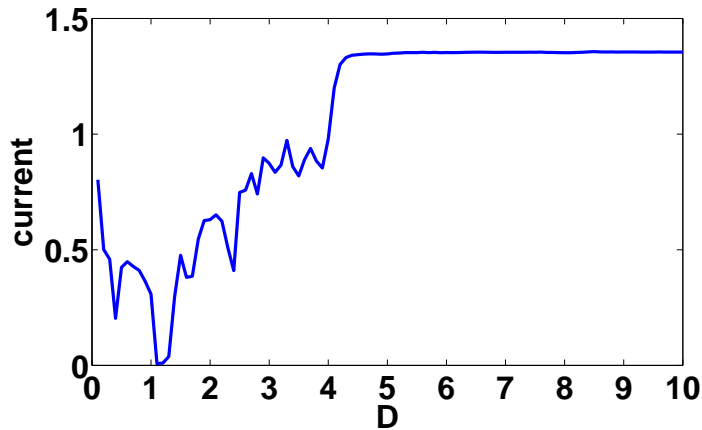


Figure 2: Current as a function of  $D$  in dimensionless units. The remaining parameter values are given by:  $\alpha = 3$ ,  $F = 0.01$  and  $q_0 = 10$ .

In the following we illustrate the complex solution behaviour of system (5),(6) and the implications for the contribution to the net current. Fig. 3 shows the temporal evolution of the coordinates  $q_1(t)$  and  $q_2(t)$  for four different values of  $D$  but for the same initial condition leading to various types of solutions. For the low value  $D = 0.5$  the coordinates perform small-amplitude oscillations around their respective starting value (see the upper left panel of Fig. 3). Thus the monomers remain trapped in the potential well and the contribution to the net current is zero. In contrast for  $D = 1$  we observe that after a finite period of

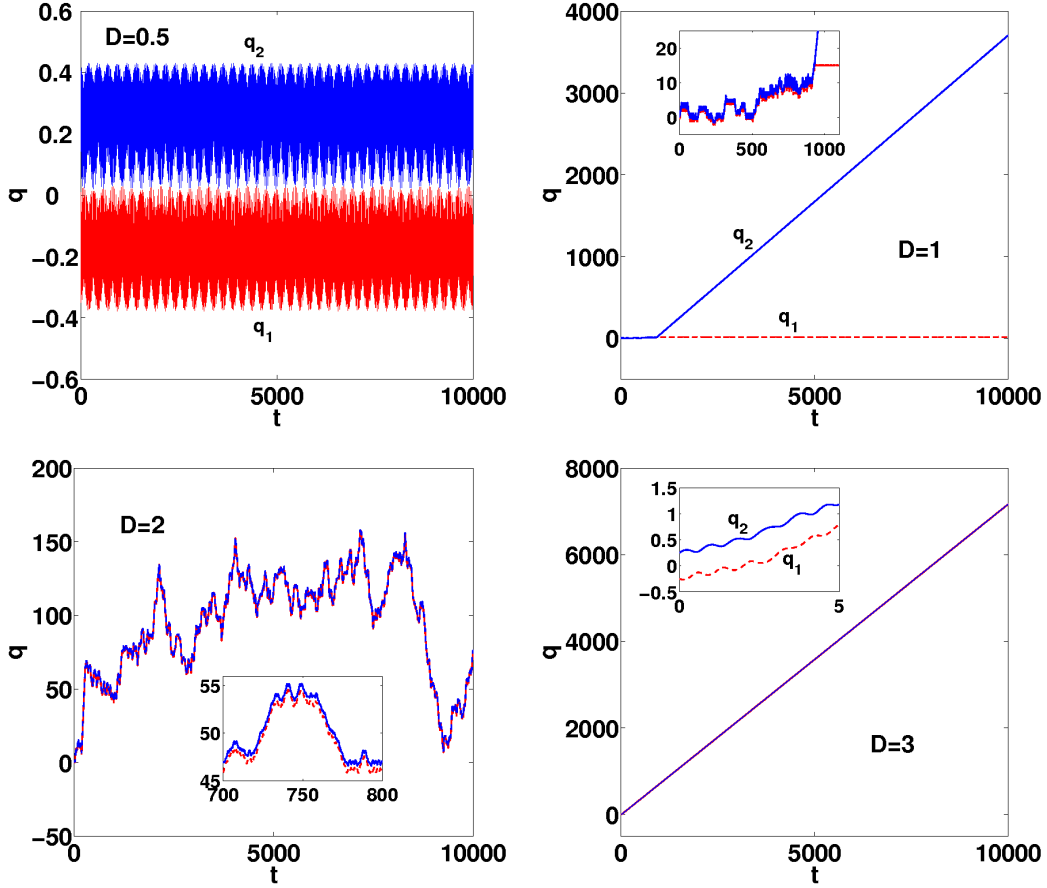


Figure 3: Four qualitatively different scenarios, illustrated by the time evolution of individual coordinates with initial conditions  $p_1(0) = -0.2100$  and  $p_2(0) = 0.4502$  for the values of  $D$  indicated in the plots. The remaining parameter values are given by:  $\alpha = 3$ ,  $F = 0.01$  and  $q_0 = 10$ . The insets show details of the evolution.

chaotic but bounded dimer motion the bond between them breaks. As a result the right monomer (with index  $n = 2$ ) is released and due to the (still acting) tilt force accelerated into the region of higher momenta while its left counterpart (with index  $n = 1$ ) becomes again trapped in a potential well. The subsequent regular dynamics is characterised by different motions of the monomers, namely that of the right monomer moving rightwards (rotations) in the asymptotic region and the left monomer performing bounded oscillations in a potential well (librations). In this case, the directed motion of the right monomer gives a contribution to the net current. We stress that, after such fragmentation, reformation of a bound state dimer from the two isolated monomers is excluded. Notice that the possibility of bond breaking allows for transient chaos [28],[29],[30].

Increasing the coupling parameter further to  $D = 2$  the chaotic coupled monomer dynamics involves irregular phases where the motion changes from forward to backward and vice versa in the manner of Lévy flights [31] in the whole simulation interval. Nevertheless the net motion proceeds to the right. Notice that the bond remains unbroken, and hence the dimer intact, in this case.

Interestingly for a high value  $D = 3$  the dimer manages quickly to escape from the potential well. (We remark that for some other initial conditions we observed first a longer transient of still bounded but chaotic motion before the escape eventually took place.) Furthermore, as the inset reveals, the two monomers perform out-of-phase motion, viz. the length of the bond between them alternately (slightly) decreases and increases. This is associated with such well-coordinated energy exchanges between the monomers that firstly the right-hand monomer overcomes the potential barrier and reaches the adjacent well on the right, subsequently the left monomer follows, and so on. We underline that prior to its arrival in the asymptotic region the trajectory passes through a chaotic transient to adopt regular dynamics in the asymptotic region. It is the asymptotic vanishing of the tilt force that makes transient chaos possible. Clearly the directed dimer motion contributes with significant weight to the net current. In particular, the dimer moves with higher velocity for  $D = 3$  than the escaped monomer does for  $D = 1$ .

To summarise briefly: we distinguish between four qualitatively different transport scenarios:

- (i) The dimer remains trapped inside the starting potential well and hence, there results no contribution to the net current.
- (ii) The dimer escapes from the starting potential and undergoes subsequently diffusive motion with no substantial contribution to the net current.
- (iii) Directed energy transfer from the left monomer to the right one leads not only to fragmentation but also to such a high energy gain of the right monomer that it can undergo directed motion to the right. This *individual* directed motion yields a considerable contribution to the net current.
- (iv) Appropriately coordinated energy redistribution between the monomers leads to directed *collective* motion such that first the right monomer performs a transition from one potential well into the next one to the right and afterwards the left monomer follows. Notice that this corresponds to repeated detrapping-trapping transitions. This scenario is optimal



in the sense that it enables both monomers to perform consecutive step-wise escapes from the potential wells. Since the total amount of energy does not suffice for a simultaneous escape of both monomers they must necessarily share their energy cooperatively in order to achieve escape at all. This almost-periodic energy exchange between the monomers corresponds in phase space to motion near a stable period-one fixed point (see further in V). Notably the directed chaotic motion persists even in the asymptotic region where there is no bias anymore. Furthermore, the resulting velocity is higher than in case (iii) and so is the contribution to the net current. We mention that, apart from the ideal situation of on-going directed motion, for other initial conditions the dimer performs directed long-distance motion in a restricted time interval at the end of which non-directed diffusive motion as in case (ii) follows.

We emphasise that the scenarios shown in Fig. 3 are not necessarily representative of the dynamics of all initial conditions at the respective values of the coupling strength  $D$ ; at  $D = 3$ , for example, scenarios (iii) and (iv) both occur (for different initial conditions). Concerning the current we therefore remark that, at each fixed value of the coupling strength  $D$ , each of the transport scenarios (i)-(iv) will, if present, contribute with different weight to the ensemble average for the current, which results in the complex behaviour seen in Fig. 2.

#### IV. PHASE SPACE DYNAMICS

In order to discuss the corresponding dynamics taking place on the three-dimensional energy hypersurface in the four-dimensional phase space we introduce the following Poincaré surface of section (PSS)

$$\Sigma = \{ p_2, q_2 | q_1 = 0, p_1 > 0 \} . \quad (10)$$

In Fig. 4(a) and (c) we depict the PSS for  $D = 0.5$  and  $D = 3$ , respectively using an ensemble of  $10^4$  initial conditions fulfilling the relation (9) with  $E_{kin} = 0.1234$ . The corresponding right panel presents the *escape time function*, defined as the time it takes the right monomer to reach the position  $q_2 = 10$ , as a function of the angle

$$\Phi = \tan^{-1}(p_2(0)/p_1(0)). \quad (11)$$

For  $D = 0.5$  there are two wide regions on the  $\Phi$ -axis for which no escape happens at all. This is the case when the monomers start with initial momenta of approximately equal

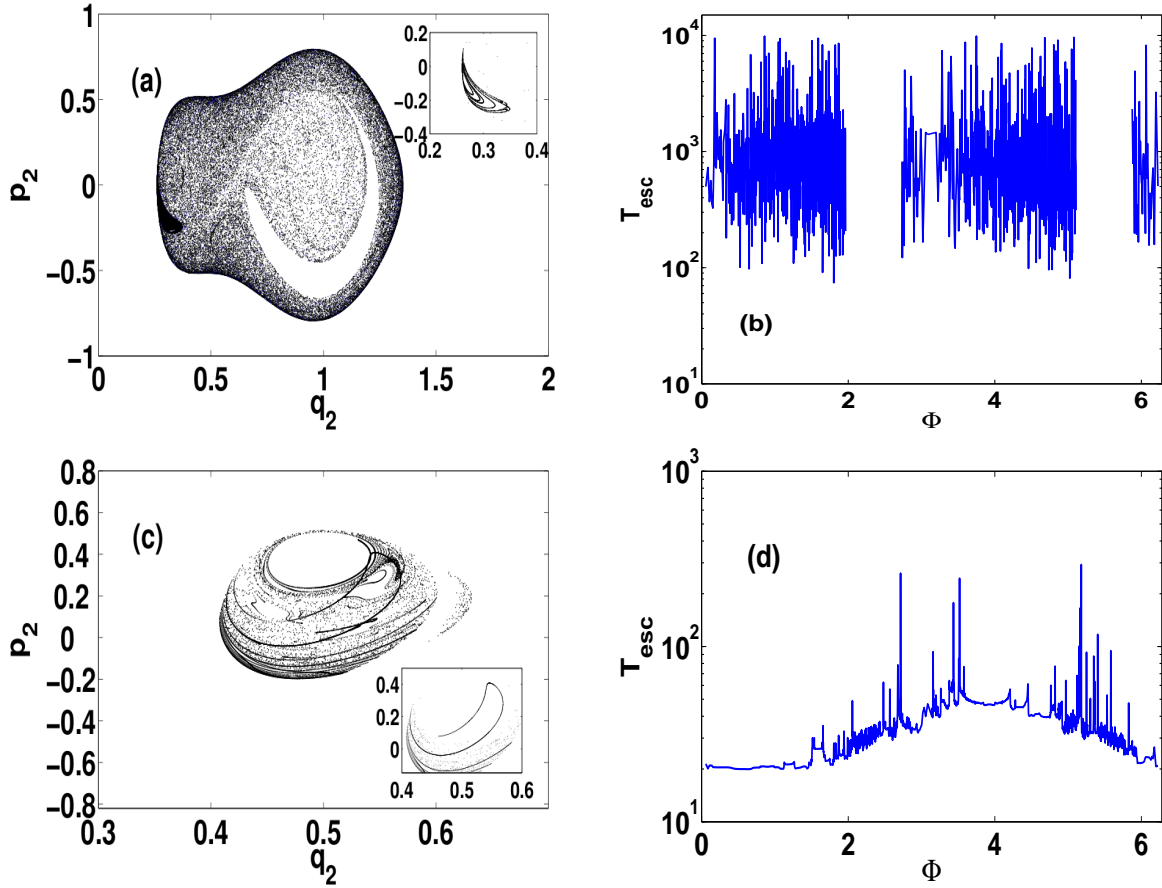


Figure 4: PSS represented in the  $p_2 - q_2$  plane (a) and (c) and escape times versus the angle  $\Phi = \tan^{-1}(p_2(0)/p_1(0))$  shown in (b) and (d). Upper (resp. lower) row:  $D = 0.5$  (resp.  $D = 3$ ). The remaining parameter values are given by:  $\alpha = 3$ ,  $F = 0.01$  and  $q_0 = 10$ . An ensemble of  $10^4$  initial conditions fulfilling relation (9) with  $E_{kin} = 0.1234$  is used.

magnitude but of opposite sign, i.e. around  $\Phi \simeq 3\pi/4$  and  $\Phi \simeq 7\pi/4$ . In both cases the resulting regular motion is associated with the stable island centered at  $(p_2, q_2) \simeq (-0.2, 0.4)$  in the corresponding PSS (displayed in the inset of Fig. 4 (a)). The physical reason for the appearance of regular trapped motion in these cases is the fact that the initial velocity of the center of mass of the dimer is virtually zero — a situation that remains virtually unchanged due to the symmetry of the washboard potential, the weakness of the tilt, and the small interaction term. An examination of the escape time function at various scales reveals that, except for the two windows of no-escape, the escape time depends sensitively on changes of the initial momenta. The trajectories attributed to escaping monomers are contained in the extended chaotic sea which densely fills the majority of the energetically-accessible regions

on the PSS (except for an infinite set of smaller islands of stability not recognisable on the scale of the PSS). A crescent-moon-shaped region within the chaotic sea remains empty on the PSS because it is not energetically accessible. In more detail, there exist chaotic invariant sets consisting of homoclinic and heteroclinic tangles which induce a fractal set of singularities into the escape time function [32]-[36]. The singularities arise at those points where the stable manifolds of unstable periodic orbits intersect the set of initial data with the effect that the corresponding trajectories become trapped for arbitrarily long times in a chaotic invariant set. It is therefore impossible to fully resolve the behaviour of the escape time function whose singularities form a fractal set with measure zero.

Interestingly, for increased coupling strength  $D = 3$  the interaction between the monomers is strong enough that fully developed chaos results and the windows of no-escape obtained in the previous case of  $D = 0.5$  vanish. In comparison, the escape times are mostly shorter by far for  $D = 3$  than for the preceding case  $D = 0.5$ . The associated PSS elucidates these differences in the escape process. (We remark that according to the condition in (10) only those trajectories for which the left monomer is still in the starting potential well contribute to the PSS.) Comparing the cases  $D = 0.5$  and  $D = 3$  one infers that in the former case the chaotic sea engulfs far more area (extending along the  $q_2$ -axis over the range of the starting potential well together with its neighbour to the right) despite the existence of the (small) stable island (inset in Fig. 4(a)). Moreover the fact that the PSS is more densely populated for  $D = 0.5$  than in the case  $D = 3$  indicates that trajectories spend longer times in the potential well(s) for  $D = 0.5$  before they manage to escape. Furthermore, for  $D = 3$  some trajectories follow directly the unstable manifold associated with a chaotic saddle appearing as a winding curve emanating from the region around  $p_2 = 0, q_2 \simeq 0.5$  (inset in Fig. 4(c)). Further details are given in Section V. This provides a mechanism for fast escape into the range of large coordinates which happens particularly for initial values lying in the range  $0 < \Phi \lesssim 1.5$ . Nonetheless there remains a large portion of trajectories that dwell for some time in the starting region before they escape in the direction of the asymptotic region. The dwell time depends sensitively on the initial conditions. On the other hand, escape does not necessarily imply sustained directed transport.

For further characterisation of the escape dynamics PSS are presented in the  $p_1 - q_1$ -plane using the intersection condition  $q_2 = 20, p_2 > 0$  yielding a snap shot of the ensemble dynamics in the asymptotic region. Note that at such a large distance from the starting point located

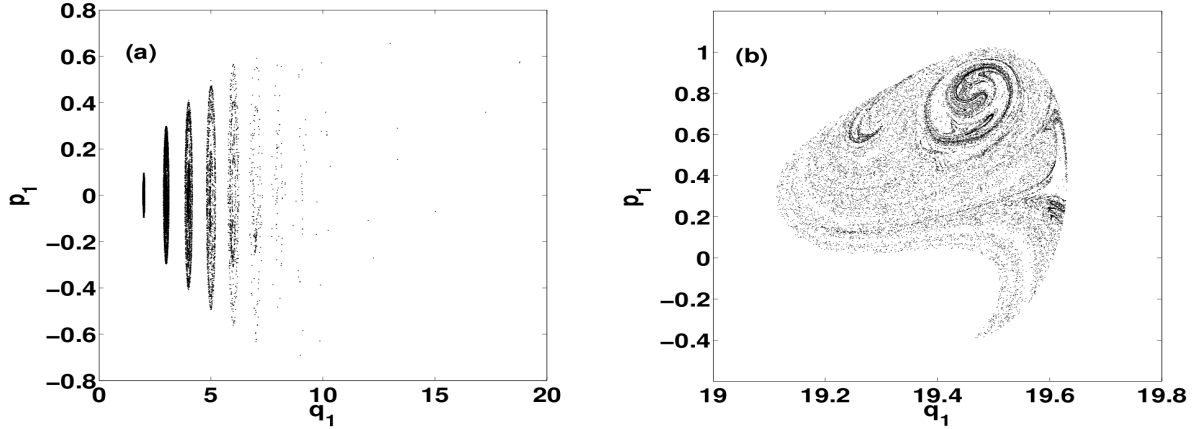


Figure 5: Sections taken when the coordinate of the right monomer reaches  $q_2 = 20$  with  $10^4$  initial conditions from an ensemble satisfying the relation (9) with  $E_{kin} = 0.1234$ . (a) (resp. (b)):  $D = 0.5$  (resp.  $D = 3$ ). The remaining parameter values are given by:  $\alpha = 3$ ,  $F = 0.01$  and  $q_0 = 10$ .

at  $q_2(0) = 0.25$ , the right monomer experiences an unbiased potential. The ensemble of initial conditions is the same as the one used for Fig. 4. The PSS for  $D = 0.5$  is depicted in Fig. 5(a) and shows that advancing right monomers leave the overwhelming majority of their left counterparts behind distributed over various potential valleys where they perform trapped motion. Clearly for the fairly low interaction potential depth  $D = 0.5$  the bond between the monomers easily breaks. In contrast, for the comparatively large interaction potential depth,  $D = 3$ , the bond between the monomers remains intact for the entire time, as seen in the right panel of Fig. 5. Hence, left monomers travel the full distance in unison with their right counterparts.

It is illustrative to consider the distribution of the momenta of the right monomers at the moment when they reach the position  $q_2 = 20$ . For  $D = 0.5$  the momenta are narrowly distributed around the peak value  $p_2 \simeq 0.92$  (not shown). In this case the particle transport is dominated by directed motion of right monomers after fragmentation (cf. scenario (iii) above). For  $D = 3$  there results a broad momentum distribution in an interval matching that covered by the  $p_1$ -values in the right panel of Fig. 5. This indicates that the dynamics in the asymptotic region involves not only directed motion but also itinerant motion as described above by the diffusive-like scenario (ii). Nevertheless the distribution of the  $p_2$  values attains a maximum at  $p_2 \simeq 0.81$ , viz. for momenta for which directed motion to the right proceeds.

## V. MOTION OF A PARTICLE IN AN EFFECTIVE TWO-DIMENSIONAL POTENTIAL

To gain further insight into the coupled monomer dynamics it is useful to perform the following canonical change of variables induced by the generating function:  $S = \frac{1}{2}(q_1 + q_2)P_x + \frac{1}{2}(q_2 - q_1)P_y$  relating the old and new variables as follows

$$p_1 = \frac{1}{2}(P_x + P_y), \quad p_2 = \frac{1}{2}(P_x - P_y), \quad (12)$$

$$Q_x = \frac{1}{2}(q_1 + q_2), \quad Q_y = \frac{1}{2}(q_2 - q_1). \quad (13)$$

The coordinate  $Q_x$  determines the position of the center of mass (CM) of the dimer, accounting for translational motion. Vibrations (V) of the dimer are described by  $Q_y$ . The Hamiltonian expressed in the new variables becomes

$$\begin{aligned} H &= \frac{1}{4}(P_x^2 + P_y^2) - \frac{1}{\pi} \cos(2\pi Q_x) \cos(2\pi Q_y) \\ &+ \frac{D}{2} (1 - \exp[-\alpha(2Q_y - l_0)])^2 \\ &- F(2Q_x - \log[\cosh(Q_x - Q_y - q_0)] - \log[\cosh(Q_x + Q_y - q_0)]) \end{aligned} \quad (14)$$

$$\equiv \frac{1}{4}(P_x^2 + P_y^2) + U(Q_x, Q_y). \quad (15)$$

The corresponding equations of motion, describing the effective motion of a particle in a two-dimensional potential landscape  $U(Q_x, Q_y)$ , are given by

$$\begin{aligned} \ddot{Q}_x &= -2 \sin(2\pi Q_x) \cos(2\pi Q_y) \\ &+ F[2 - \tanh(Q_x - Q_y - q_0) - \tanh(Q_x + Q_y - q_0)] \\ \ddot{Q}_y &= -2 \cos(2\pi Q_x) \sin(2\pi Q_y) \\ &- 2\alpha D(1 - \exp[-\alpha(2Q_y - l_0)]) \exp[-\alpha(2Q_y - l_0)] \\ &+ F[\tanh(Q_x - Q_y - q_0) - \tanh(Q_x + Q_y - q_0)]. \end{aligned} \quad (16)$$

For  $Q_x, Q_y \ll q_0$  the impact of the external tilt force matters only in the first equation whereas the Morse coupling enters only in the second equation. The interaction between the  $Q_x$  (CM) and  $Q_y$  (V) degree of freedom (d.o.f.) results from parametric modulations of the respective washboard potential force term. The effective potential  $U(Q_x, Q_y)$  is displayed in Fig. 6 for the interaction potential depths  $D = 0.5$  and  $D = 3$  respectively. The superimposed trajectory, corresponding to the dynamics shown in Fig. 3 (a) and (c) respectively,

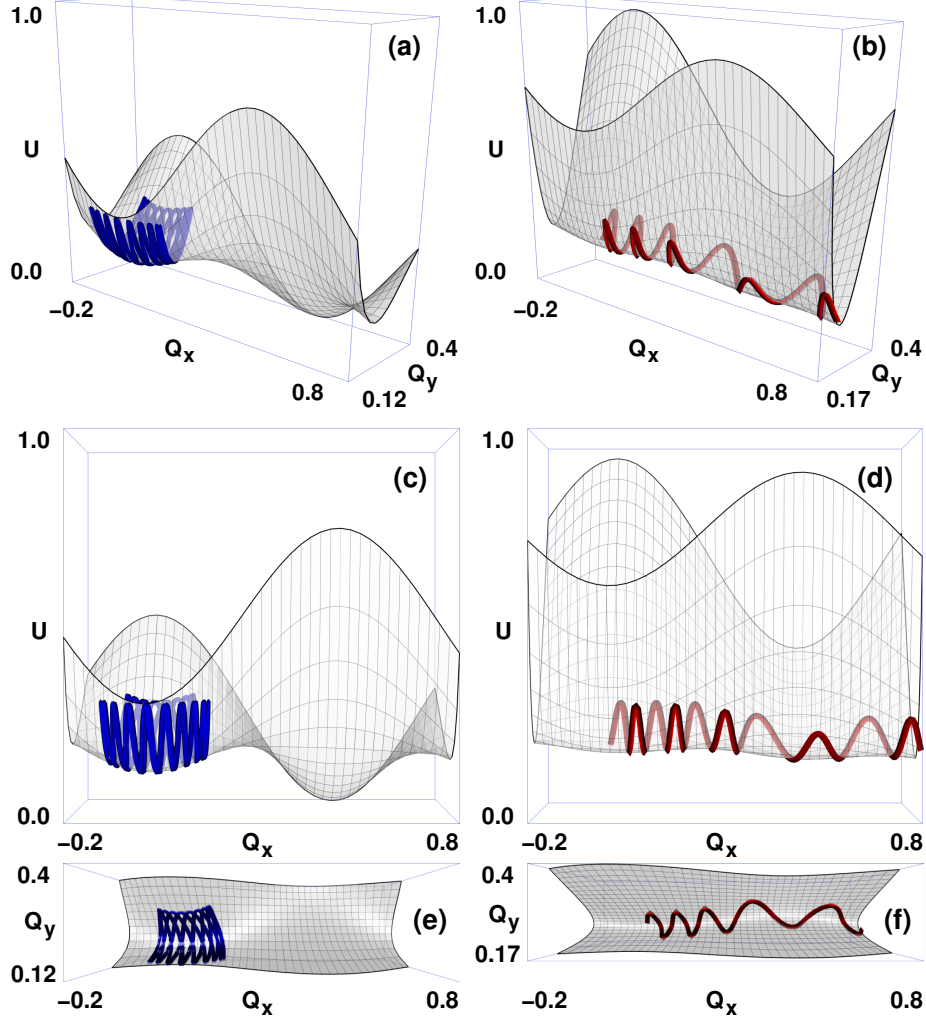


Figure 6: (Colour online) Evolution of the trajectory in the two-dimensional potential energy landscape  $U(Q_x, Q_y)$ . The parameter values are  $l_0 = 0.5$ ,  $\alpha = 3$ . Left panels (a,c,e): trapped particle for  $D = 0.5$  and right panels (b,d,f): moving particle for  $D = 3$ . For clarity, the middle (c,d) and bottom (e,f) rows show profile views ( $Q_x, U$ ) and plan views ( $Q_x, Q_y$ ), respectively. The steepness of the potential surface in the case  $D = 3$  (b,d,f) necessitates plotting the potential surface for a slightly smaller  $Q_y$  range. The left and right panels are shown to the same scale in each case.

starts close to the potential minimum for  $D = 0.5$  situated at  $(Q_x, Q_y) = (0.014, 0.173)$ . The corresponding state of lowest energy is denoted by  $E_g$ . There exists a nearby saddle, aforementioned in Section IV, which for  $D = 0.5$  is located at  $(Q_x, Q_y) = (0.241, 0.244)$  having energy  $U_s$ . In order to advance towards higher  $Q_x$ -values in the two-dimensional potential landscape the particle needs to overcome a potential barrier the height of which is determined by  $\Delta U = U_s - U_g$ . Apparently for  $D = 0.5$  the trajectory remains trapped inside the

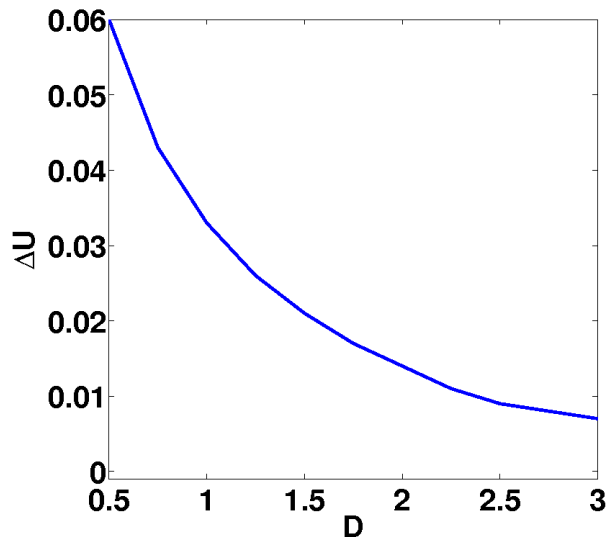


Figure 7: (Colour online) Difference between the energy of the potential minimum and the nearby saddle as a function of  $D$ . The remaining parameter values are  $l_0 = 0.5$ ,  $q_0 = 10$ ,  $F = 0.01$ , and  $\alpha = 3$ .

potential well (cf. Fig. 3 (a)). This is mainly connected with the relatively large-amplitude excursions in the  $Q_y$ -direction pointing to rather pronounced bond stretching/compression. In fact, the major part of the total energy is contained in the Morse interaction term, viz. in the V-d.o.f., amounting to 70%. Thus there remains little energy that can flow into the CM-d.o.f., hampering the translational motion necessary to overcome the potential barrier. In contrast for  $D = 3$ , when the bond between the monomers is more rigid by far than before, the Morse bond energy constitutes only a small amount of the total energy. As a consequence the CM-d.o.f. possesses enough energy that the trajectory easily overcomes the potential barrier and passes from one well to a neighbouring one (right panel in Fig. 6). Moreover, along the line  $Q_y = 0.25$ , that is  $-q_1 = q_2 = 0.25$ , there is no gradient of the potential in the  $Q_x$ -direction (CM motion direction). Therefore a strong enough interaction strength  $D$  is advantageous for transport because it confines the motion of the dimer along a narrow strip centered along the line  $Q_y = 0.25$ . At the same time the height of the energy barrier  $\Delta U$  decreases with increasing interaction potential depth as illustrated in Fig. 7. Conclusively, motion of the mean coordinate  $Q_x$  from one potential well into the neighbouring one is readily accomplished for large values of  $D$  which is reflected in a high current (see Fig. 2 above).

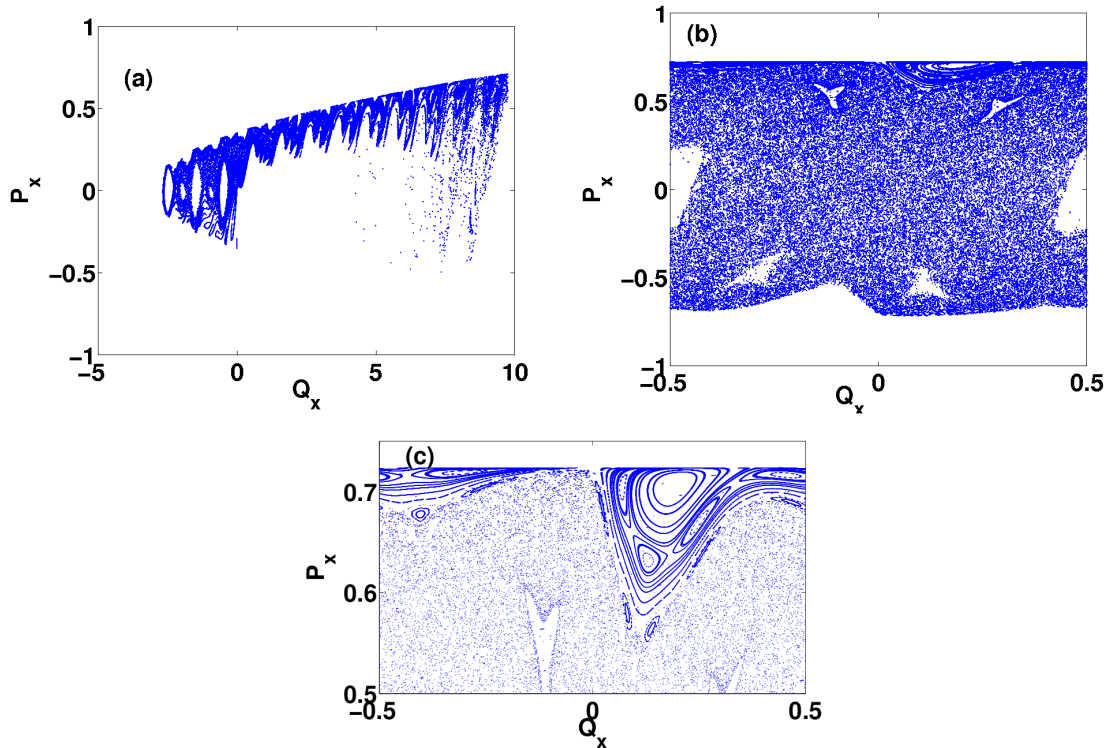


Figure 8: (Colour online) PSS for the dynamics corresponding to a symmetrical uniform distribution of initial conditions satisfying relation (9) in the potential well at  $Q_x = 0$ , showing (a)  $Q_x \leq 10$  and (b) the asymptotic regime  $Q_x > 10$  (shown mod (1)), for coupling parameter  $D = 3$ . The remaining parameter values are  $\alpha = 3$ ,  $F = 0.01$  and  $q_0 = 10$ . The panel (c) shows detail of the mixed phase space at the upper boundary of the chaotic layer in (b).

Finally, we relate the escape process and the emergence of directed chaotic motion to the phase space structure of the transformed system with Hamiltonian given in Eq. (15). To this end we use the following PSS

$$\Sigma = \{ P_x, Q_x | Q_y = 1/4, P_y > 0 \} . \quad (17)$$

In Fig. 8 we plot for a strong particle coupling  $D = 3$  the PSS corresponding to the escape dynamics when  $Q_x \leq 10$  and the dynamics in the asymptotic region, i.e.  $Q_x > 10$  (for those trajectories which reach it), in (a) and (b) respectively, being characterised by chaotic sets. (In Fig. 8 (b) the coordinate  $Q_x$  is presented mod(1).) In Fig. 8 (a) chaotic saddles, formed by the intersecting stable and unstable manifolds of unstable periodic points, govern the dynamics. The majority of escaping trajectories follows the unstable manifold of the saddle point located at  $(Q_x, Q_y) = (0.188, 0.243)$ . On the other hand there are trajectories



that remain in the starting region or spend at least some time there before escape as a consequence of the presence of chaotic saddles [37],[38]. Furthermore, on approaching the asymptotic region, where the tilt of the washboard potential vanishes, some of the previously-escaping dimers become trapped in wells of the washboard potential again.

From Fig. 8 (b), depicting the PSS in the asymptotic region, we conclude that the bulk of the layer on the PSS is covered by a chaotic set. Within the chaotic set trajectories move in a diffusive way with changes of the direction of motion not contributing to transport. Notably, at the upper boundary of the layer, shown in Fig. 8 (c), islands of regular motion arise from those trajectories that have settled on regular dynamics after their passage through a chaotic transient. Most importantly, these islands possess non-zero winding numbers and thus act as ballistic channels [39] providing directed transport to the right. In particular, the dynamics within the island structure centered at the stable period-one fixed point  $(P_x, Q_x) = (0.703, 0.180)$  reflects the almost-synchronous monomer motion described in scenario (iv) in Section III. In more detail, motion near the fixed point corresponds to almost-periodic energy exchange between the monomers which is connected with only minor bond deformations which corroborates the findings reported above for the optimal transport scenario.

## VI. SUMMARY

We have analysed the Hamiltonian dynamics of two nonlinearly coupled particles evolving in a washboard potential. Notably the total energy does not suffice to enable simultaneous escape of the two particles, initially trapped in a well of the washboard potential. Due to appropriate energy redistribution, at least one of the particles can achieve escape. (See also [40].) Ideally the two particles share energy almost periodically in such a way that consecutive detrapping-trapping transitions take place during which the particles escape one after another from one well into an adjacent one. It has been demonstrated that a weak tilt force, vanishing asymptotically in the direction of the bias, is sufficient to instigate directed motion of the escaping particles. Transport is accomplished for those trajectories which follow a chaotic transient, associated with the dynamics of chaotic saddles, settling afterwards on regular motion. The key mechanism of current rectification is based on the asymptotically vanishing tilt causing a symmetry breaking of the non-chaotic fraction of the dynamics where only at the upper boundary of the chaotic layer resonance islands appear.

The latter is supported by transporting island structures in the mixed phase space which serve for long-range directed transport.

Finally, we mention that it is certainly interesting to extend the study of directed motion to systems involving many more degrees of freedom than in the current dimer case where the dynamics within transporting islands can be investigated utilising two-dimensional Poincaré surface of sections. In particular, it needs to be examined what structures in higher dimensional phase spaces play the role of possible ballistic channels providing directed collective transport.

- 
- [1] L.P. Faucheux, G. Stolovitzky, and A. Libchaber, *Phys. Rev. E* **51**, 5239 (1995).
  - [2] P.E. Parris, M. Kus, D.H. Dunlap, and V.M. Kenkre, *Phys. Rev. E* **56**, 5295 (1997).
  - [3] G. Constantini and F. Marchesoni, *Eur. Phys. Lett.* **48**, 491 (1999).
  - [4] P. Reimann *et al*, *Phys. Rev. Lett.* **87**, 010602 (2001).
  - [5] D. Reguera *et al*, *Eur. Phys. Lett.* **57**, 644 (2002).
  - [6] S.A. Tatarkova, W. Sibbett, and K. Dholakia, *Phys. Rev. Lett.* **91**, 038101 (2003).
  - [7] O.M. Braun, R. Ferrando, and G.E. Tommei, *Phys. Rev. E* **68**, 051101 (2003).
  - [8] E. Heinsalu, M. Patriarca, and F. Marchesoni, *Phys. Rev. E* **77**, 021129 (2008).
  - [9] E. Pijper and A. Fasolino, *Phys. Rev. B* **72**, 165328 (2005).
  - [10] S.H. Lee and D.G. Grier, *Phys. Rev. Lett.* **96**, 190601 (2006).
  - [11] J. Regtmeier *et al*, *Anal. Chem.* **79**, 3925 (2007).
  - [12] F. Jülicher, A. Ajdari, and J. Prost, *Rev Mod. Phys.* **69**, 1269 (1997).
  - [13] P. Reimann, *Phys. Rep.* **361**, 57 (2002).
  - [14] A. Barone and G. Paternó, *Physics and Applications of the Josephson Effect*, (Wiley, New York, 1982).
  - [15] G. Gruner, A. Zawadowski, and P.M. Chaikin, *Phys. Rev. Lett.* **46**, 511 (1981).
  - [16] P. Fulde, L. Pietronero, W.R. Schneider, and S. Strässler, *Phys. Rev. Lett.* **35**, 1776 (1975).
  - [17] D. Reguera, J.M. Rubí, and A. Pérez-Madrid, *Phys. Rev. E* **62**, 5313 (2002).
  - [18] C.W. Lindsey, *Synchronization Systems in Communication and Control* (Prentice-Hall, Englewood Cliffs, New Jersey, 1972).
  - [19] J.W.M. Frenken and J.F. Van Der Veen, *Phys. Rev. Lett.* **54**, 34 (1985).

- [20] O.M. Braun, Surf. Sci. **230**, 262 (1990).
- [21] M. Partriarca and P. Szelestey, Act. Phys. Pol. **36**, 1745 (2005).
- [22] C. Fusco and A. Fasolino, Thin Solid Films **428**, 34 (2003).
- [23] S. Goncalves, V.M. Kenkre, and A.R. Bishop, Phys. Rev. B **70**, 195415 (2004).
- [24] M. Evstigneev, S. von Gehlen, and P. Reimann, Phys. Rev. E **79**, 011116 (2009).
- [25] P. Reimann, R. Kawai, C. Van den Broeck, and P. Hänggi, Europhys. Lett. **45**, 545 (1999).
- [26] D. Hennig, L. Schimansky-Geier, and P. Hänggi, Europhys. Lett. **83**, 60008 (2008).
- [27] S. Martens, D. Hennig, S. Fugmann, and L. Schimansky-Geier, Phys. Rev. E **78** 041121 (2008).
- [28] T. Tel, in *Directions in Chaos* (Ed.: Bai-lin Hao, World Scientific, Singapore, Vol. 3, 1990).
- [29] T. Tel and M. Gruiz *Chaotic Dynamics* Cambridge University Press, Cambridge, 2006).
- [30] M. Zaslavsky, *Chaos in Dynamical Systems* (Harwood, New York, 1985), *Physics of Chaos in Hamiltonian Systems* (Imperial College Press, London, 1998).
- [31] O.M. Yevtushenko and K. Richter, Physica E **4**, 256 (1999); M. Glück, A.R. Kolovsky, and H.-J. Korsch, Physica D **116**, 283 (1998).
- [32] E. Ott *Chaos in Dynamical Systems* (University of Cambridge, Cambridge, 1992).
- [33] S. Wiggins, *Chaotic Transport in Dynamical Systems* (Springer-Verlag, New York, 1992).
- [34] B. Ruckerl and C. Jung, J. Phys. A **27**, 6741 (1994).
- [35] A. Emmanouilidou, C. Jung, and L.E. Reichl, Phys. Rev. E **68**, 046207 (2003).
- [36] A.M. Barr, Kyungsun Na, and L.E. Reichl, Phys. Rev. E **79**, 026215 (2009).
- [37] C. Grebogi, E. Ott, and J.A. Yorke, Physica D **7**, 181 (1983); S. Bleher, C. Grebogi, E. Ott, and R. Brown, Phys. Rev. A **38**, 930 (1988); S. Bleher, C. Grebogi, and E. Ott, Physica D **46**, 87 (1990).
- [38] K.T. Alligood, T.D. Sauer, and J.A. Yorke *Chaos, An Introduction to Dynamical Systems* (Springer-Verlag, New York, 1997).
- [39] S. Denisov and S. Flach, Phys. Rev. E **64**, 056236 (2001); S. Denisov, J. Klafter, M. Urbakh, and S. Flach, Physica D **170**, 131 (2002); S. Denisov, J. Klafter, and M. Urbakh, Phys. Rev. E **66**, 046217 (2002); D. Hennig, L. Schimansky-Geier, and P. Hänggi, Eur. Phys. J. B **62**, 493 (2008).
- [40] S. Fugmann, D. Hennig, S. Martens, and L. Schimansky-Geier, Physica D **237**, 3179 (2008).